Quantum Chemical and Kinetic Study of the Oxidation Mechanisms of Naphthalene Initiated by Hydroxyl Radicals. I. The OH Addition Pathway

Abolfazl Shiroudi[†], Michael S. Deleuze[†] and Sébastien Canneaux[‡]
[†]Center of Molecular and Materials Modelling, Hasselt University, Agoralaan, Gebouw D, B-3590 Diepenbeek, Belgium
[‡]Université Lille1 Sciences et Technologies, Cité scientifique, 59655 Villeneuve d'Ascq Cedex, France

1. INTRODUCTION

The gas-phase reaction between hydroxyl radicals and naphthalene has been experimentally studied at $T < 410$ K and at temperatures ranging from 636 to 873 K, by means of laser flash photolysis using laser-induced fluorescence, at pressures comprised between 6 and 128 mbar, under inert (He) conditions. An Arrhenius plot of all the kinetic rate constants that were measured or inferred so far under such conditions is depicted in Figure 1.

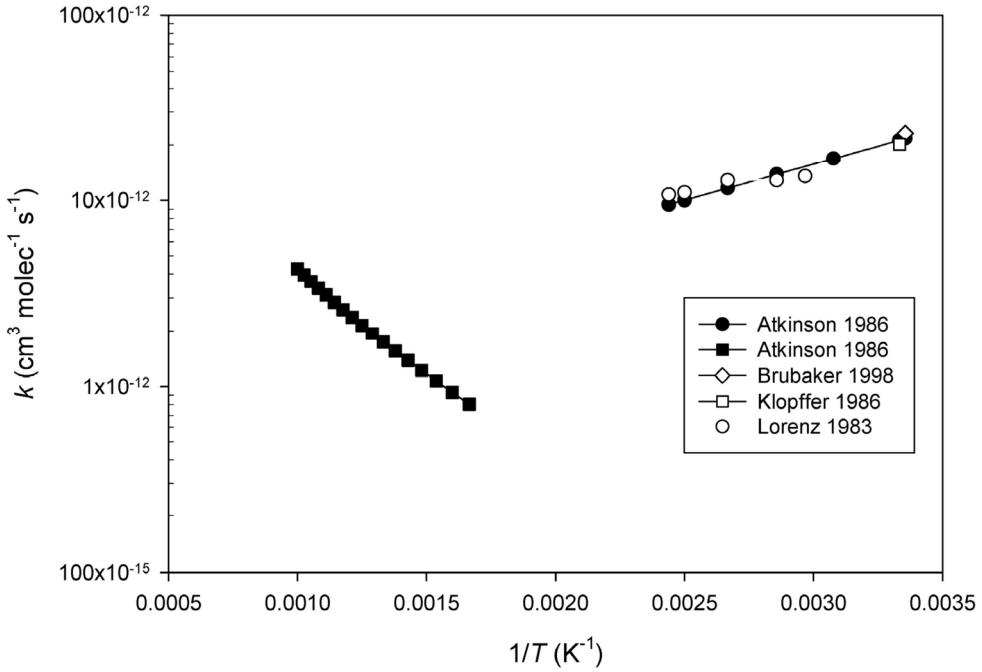

Figure 1. Arrhenius plot of the rate constants for the reaction of OH radicals with naphthalene:

Different energy barriers obviously prevail at $T < 410$ K and at $T > 636$ K. Two different chemical reaction pathways, referred to as the OH addition and H abstraction pathways, respectively, have been suggested to explain such features:

$$C_{10}H_8 + OH^\bullet \underset{k_{-1}}{\overset{k_1}{\rightleftarrows}} [C_{10}H_8OH]^\bullet$$

$$[C_{10}H_8OH]^\bullet \xrightarrow{k_2} C_{10}H_7OH + H^\bullet \quad ; \quad (T \le 410\ \text{K})$$

$$[C_{10}H_8OH]^\bullet \xrightarrow{k_2'} C_{10}H_7^\bullet + H_2O \quad ; \quad (T \ge 600\ \text{K})$$

At $T < 410$ K, the addition of the hydroxyl radical to naphthalene starts with the formation of a pre-reactive molecular complex, IM1 (Figure 2). The reaction proceeds in two steps, involving a fast and reversible reaction between the OH radical and naphthalene to form an energized adduct $[C_{10}H_8OH]^{\bullet}$ (IM2), followed by an irreversible step, corresponding to the unimolecular dissociation of this adduct into 1- or 2-naphthol and one H-atom ($H^{\bullet}$). It has been experimentally observed that, at $T < 410$ K, the production of 1-naphthol (**P1**) is favored by a ratio 2:1 over 2-naphthol (**P2**).

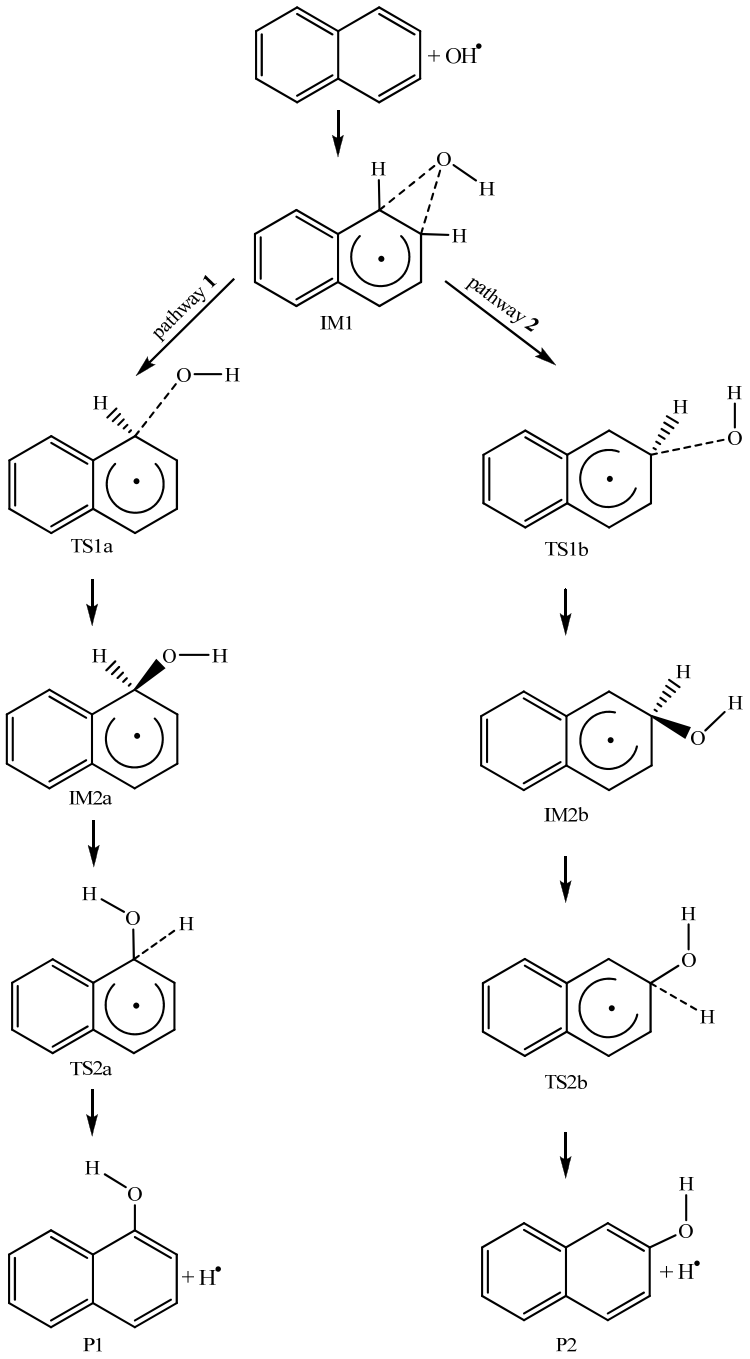

Figure 2. Reaction pathways for the oxidation of naphthalene by hydroxyl radicals.

2. COMPUTATIONAL DETAILS

Our most accurate calculations were conducted at the CBS-QB3 level of theory, which involves the following steps:

– B3LYP/6-311G(2d,d,p) geometry optimization.
– B3LYP/6-311G(2d,d,p) frequency calculation with a 0.99 scale factor for the ZPE.
– CCSD(T)/6-31+G* energy calculation.
– MP4(SDQ)/6-31+G(d(f),p) energy calculation.
– UMP2/6-311+G(3d2f,2df,2p) energy calculation and extrapolation to a complete basis set.

The CBS-QB3 approach is known to yield mean absolute deviation of 1.1 kcal mol^{-1} on the G2/97 test set for reaction energies. This approach includes a correction for spin contamination in open-shell species. Thermodynamic state functions were computed at the RRHO level. The rate constants and the branching ratios for each reaction channel were evaluated using transition state theory (TST) using CBS-QB3 values for activation energies, and B3LYP/6-311G (2d,d,p) partition functions:

$$k_{TST} = \kappa(T)\frac{\sigma k_B T}{h} V_m(T) \frac{Q^{\neq}_{TS}(T)}{Q_A(T).Q_B(T)} \exp(-E_a/RT) \quad \text{(for bimolecular reactions)} \quad (1)$$

$$k_{TST} = \kappa(T)\frac{\sigma k_B T}{h} \frac{Q^{\neq}_{TS}(T)}{Q_A(T)} \exp(-E_a/RT) \quad \text{(for unimolecular reactions)} \quad (2)$$

along with $\kappa(T)$ a relevant (Eckart) tunneling correction factor.

Statistical Rice-Ramsperger-Kassel-Marcus (RRKM) has been used along with the strong collision approximation in order to evaluate pressure effects on a microcanonical basis, both in the fall-off regime and towards the high pressure limit (scaling factor of 0.99 on the B3LYP/6-311G(2d,d,p) frequencies, collisional efficiency β_c=0.2, LJ parameters for naphthalene: σ = 6.45 Å, ε/k_B = 554.4 K, LJ parameters the naphthol radical: σ = 6.57 Å, ε/k_B = 612.7 K, LJ parameters for helium (diluent gas): σ = 2.28 Å and ε/k_B = 10.2 K).

Assuming a steady state regime, we have:

$$k_{R\rightarrow IM2x} = \frac{k_{IM1\rightarrow R} \times K_c \times k_{IM1\rightarrow IM2x}}{k_{IM1\rightarrow R} + k_{IM1\rightarrow IM2x}} \quad (3)$$

where $k_{IM1\rightarrow R}$ and $k_{IM1\rightarrow}k_{IM2x}$ (x=a,b) represent reverse and forward unimolecular reaction rate constants (in s^{-1}).

3. RESULTS AND DISCUSSION

3.1. Energetic and thermodynamic parameters

In line with experimental Arrhenius activation energies of –1.27 kcal mol^{-1} or –1.8 kcal mol^{-1}, our calculations locate the transition state TS1a on pathway **1** at 0.6 to 3.9 kcal mol^{-1} below the reactants. Our CBS-QB3) estimate for the corresponding activation energy amounts

to −1.5 kcal mol^{-1}. On the other hand, at this level, the transition state TS1b on pathway **2** is located at 1 kcal mol^{-1} above the reactants.

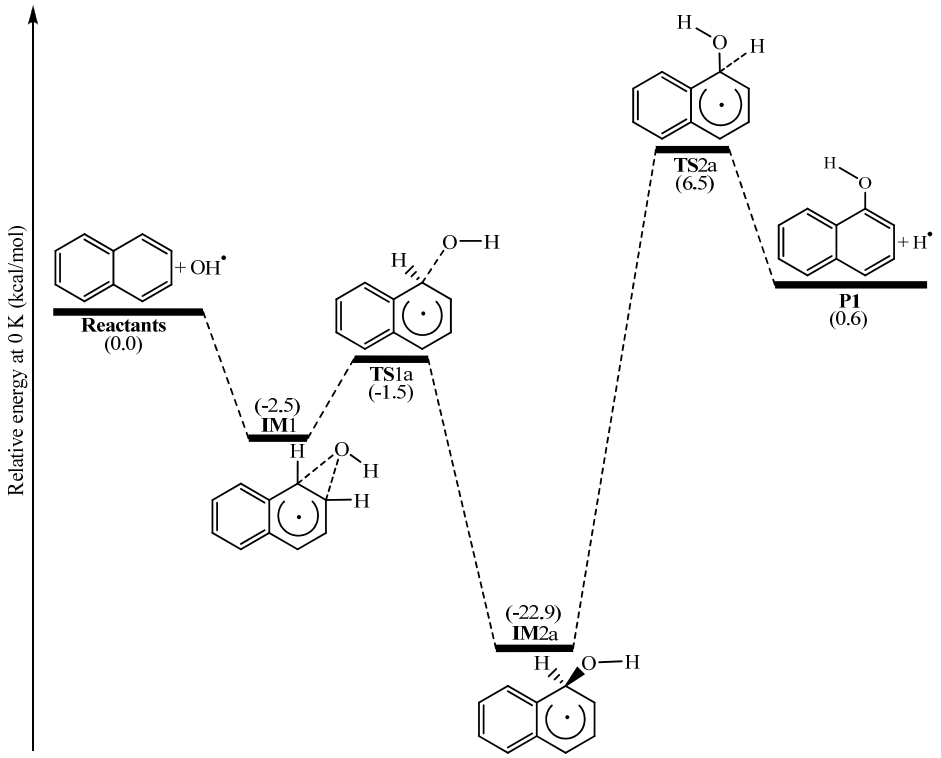

Figure 3. CBS-QB3 energy profile for the reaction pathway **1** characterizing the oxidation of naphthalene by OH radicals into 1-naphthol.

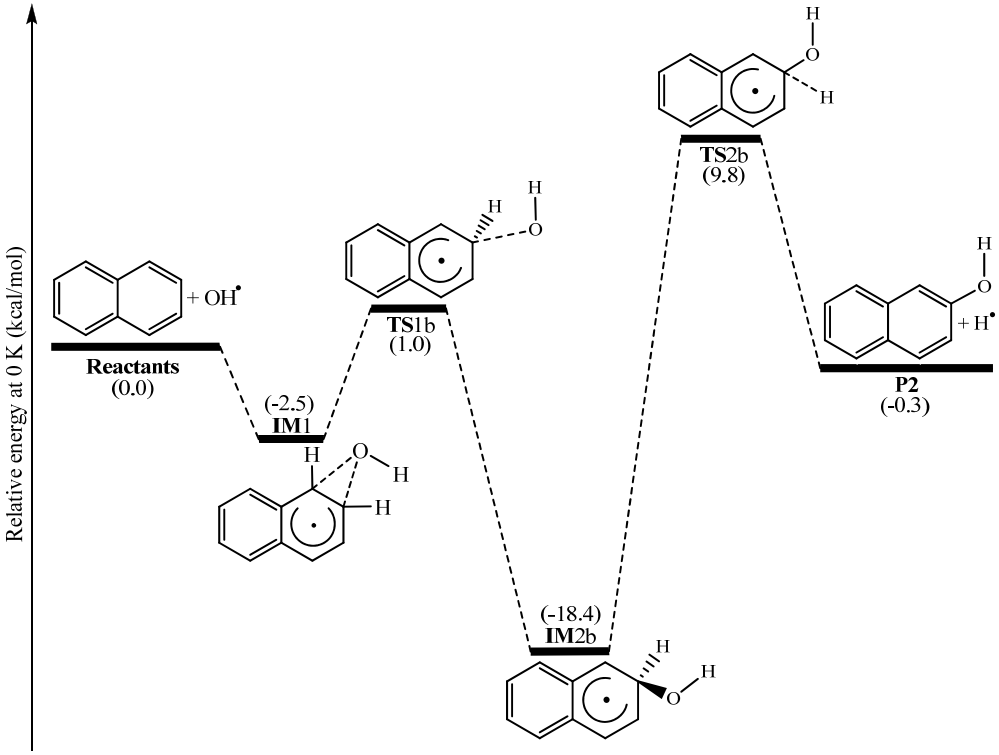

Figure 4. CBS-QB3 energy profile for the reaction pathway **2** characterizing the oxidation of naphthalene by OH radicals into 2-naphthol.

TS1a and TS1b are characterized by NICS indices equal to −15.43 and −13.56, respectively. Evidently, the more pronounced aromatic nature of TS1a explains its higher stability, compared with TS1b. Also, the lower energy of IM2a compared with IM2b reflects the more strongly pronounced aromatic nature of the former energized adduct: indeed, IM2a and IM2b are characterized by NICS indices equal to −3.94 and −1.28, respectively.

Pathway **1** (R→P1) is an endothermic process (ΔH= 1 kcal mol^{-1}), whereas pathway **2** (R→P2) is slightly exothermic (ΔH= −0.1 kcal mol^{-1}). Both pathways are found to be endergonic processes ($\Delta G > 0$) at ambient temperature and pressure.

Leffler-Hammond's postulate states that the structure of a transition state resembles that of the species nearest to it in free energy. This can be quantified in terms of the position of the transition structure along the reaction coordinate, n_T:

$$n_T = \frac{1}{2-(\Delta G_r / \Delta G^{\neq})} \tag{4}$$

For IM2a→P1, n_T = 0.71. For IM2b→P2, n_T = 0.64. In line with the energy profiles and structural observations, the TS1x transition structures (x=a,b) are thus more similar to the pre-reactive complexes, whereas the TS2x transition structures are more similar to the products.

3.2. Kinetic parameters

TST and RRKM estimates for rate constants are listed in Tables 1 and 2 along with experimental data, at temperatures ranging from 300 to 407 K.. On the experimental side, rate constants were obtained by monitoring continuously the concentration of hydroxyl radical at the entrance of the reaction cell using UV absorption. These rate constants must correspond therefore to the first bimolecular reaction step (R→IM2x , x=a,b).

The fact that the first bimolecular reaction step on pathway **1** is characterized by a slightly negative energy barrier whereas on pathway **2** it is characterized by a small positive energy barrier is not sufficient to explain why the production of 1-naphthol was experimentally found to be favored with respect to the production of 2-naphtol. A safer explanation also implies calculations of effective kinetic rate constants that account for the second unimolecular dissociation reaction step. Indeed, TST and RRKM results indicate that, at P = 1 bar, the post-reactive intermediate IM2b decomposes ~10 times faster than IM2a.

In order to evaluate effective rate constants, we assume that the kinetics of the reaction can be modelled according to a two-step mechanism:

$$\text{step 1: } C_{10}H_8 + OH^{\bullet} \underset{k_{IM2x\rightarrow R}}{\overset{k_{R\rightarrow IM2x}}{\rightleftharpoons}} [C_{10}H_8OH]^{\bullet}$$

$$\text{step 2: } [C_{10}H_8OH]^{\bullet} \xrightarrow{k_{IM2x\rightarrow P1/P2}} C_{10}H_7OH + H^{\bullet}$$

A steady-state analysis upon the above sequence leads to the following effective rate constants characterizing pathways **1** and **2**:

$$k_{eff}(1) = \frac{k_{R\rightarrow IM2a}\, k_{IM2a\rightarrow P1}}{k_{IM2a\rightarrow R} + k_{IM2a\rightarrow P1}} \tag{5}$$

$$k_{eff}(2) = \frac{k_{R\rightarrow IM2b}\, k_{IM2b\rightarrow P2}}{k_{IM2b\rightarrow R} + k_{IM2b\rightarrow P2}} \tag{6}$$

Table 1. Rate constants (units: unimolecular reactions in s^{-1}; bimolecular reactions in cm^3 $molecule^{-1}$ s^{-1}), effective rate constants, and branching ratios for the reported reaction channels by means of TST theory (P = 1 bar), according to the computed CBS-QB3 energy profiles (see methodology section for details).

T (K)	Rate constant						Effective rate constant		Branching ratio		k_{exp} [9,14,18]
	R→IM2a	R→IM2b	IM2a→R	IM2b→R	IM2a→P1	IM2b→P2	R→P1	R→P2	R(1)	R(2)	
300	4.49×10^{-14}	7.91×10^{-15}	3.12×10^{-2}	4.98×10^{-1}	2.76×10^{-6}	2.90×10^{-5}	3.97×10^{-18}	4.61×10^{-19}	89.61	10.39	$(18.6\pm1.0)\times10^{-12}$
337	3.74×10^{-14}	1.41×10^{-14}	1.57×10^{0}	1.47×10^{1}	2.65×10^{-4}	2.18×10^{-3}	6.31×10^{-18}	2.09×10^{-18}	75.12	24.88	$(14.6\pm5.0)\times10^{-12}$
358	3.46×10^{-14}	1.87×10^{-14}	8.90×10^{0}	7.55×10^{1}	2.37×10^{-3}	1.72×10^{-2}	9.21×10^{-18}	4.26×10^{-18}	68.38	31.62	$(11.0\pm4.4)\times10^{-12}$
378	3.26×10^{-14}	2.40×10^{-14}	3.78×10^{1}	3.11×10^{2}	1.51×10^{-2}	9.84×10^{-2}	1.30×10^{-17}	7.59×10^{-18}	63.17	36.83	$(10.1\pm4.0)\times10^{-12}$
407	3.06×10^{-14}	3.33×10^{-14}	2.38×10^{2}	1.96×10^{3}	1.56×10^{-1}	9.08×10^{-1}	2.00×10^{-17}	1.54×10^{-17}	56.52	43.48	$(10.5\pm4.0)\times10^{-12}$

Table 2. Rate constants (units: unimolecular reactions in s^{-1}; bimolecular reactions in cm^3 $molecule^{-1}$ s^{-1}), effective rate constants, and branching ratios for the reported reaction channels by means of RRKM theory (P = 1 bar), according to the computed CBS-QB3 energy profiles (see methodology section for details).

T (K)	Rate constant						Effective rate constant		Branching ratio		k_{exp} [9,14,18]
	R→IM2a	R→IM2b	IM2a→R	IM2b→R	IM2a→P1	IM2b→P2	R→P1	R→P2	R(1)	R(2)	
300	2.92×10^{-14}	4.65×10^{-15}	2.87×10^{-2}	4.91×10^{-1}	1.47×10^{-6}	1.37×10^{-5}	1.50×10^{-18}	1.30×10^{-19}	92.02	7.98	$(18.6\pm1.0)\times10^{-12}$
337	2.48×10^{-14}	6.76×10^{-15}	1.28×10^{0}	1.57×10^{1}	1.59×10^{-4}	1.19×10^{-3}	3.08×10^{-18}	5.12×10^{-19}	85.74	14.26	$(14.6\pm5.0)\times10^{-12}$
358	2.31×10^{-14}	7.93×10^{-15}	7.86×10^{0}	8.22×10^{1}	1.48×10^{-3}	1.00×10^{-2}	4.35×10^{-18}	9.65×10^{-19}	81.85	18.15	$(11.0\pm4.4)\times10^{-12}$
378	2.19×10^{-14}	9.02×10^{-15}	3.67×10^{1}	3.35×10^{2}	9.92×10^{-3}	6.13×10^{-2}	5.89×10^{-18}	1.65×10^{-18}	78.12	21.88	$(10.1\pm4.0)\times10^{-12}$
407	2.03×10^{-14}	1.04×10^{-14}	2.63×10^{2}	2.02×10^{3}	1.13×10^{-1}	6.23×10^{-1}	8.76×10^{-18}	3.21×10^{-18}	73.21	26.79	$(10.5\pm4.0)\times10^{-12}$

RRKM data indicate that, from 1 bar down to pressures of 0.01 mbar, $k_{IM2a\rightarrow P1}$ and $k_{IM2b\rightarrow P2}$ are much smaller than $k_{IM2a\rightarrow R}$ and $k_{IM2b\rightarrow R}$, respectively, and can thus be neglected from the above denominators. This implies that, at pressures larger than 0.01 mbar:

$$k_{eff}(1) = K_c(1)\, k_{IM2a\rightarrow P1} \quad (7)$$

$$k_{eff}(2) = K_c(2)\, k_{IM2b\rightarrow P2} \quad (8)$$

where $K_c(1)$ and $K_c(2)$ are the relevant equilibrium constants for the pre-equilibrium between the reactants and the energized adducts:

$$K_c(1) = \frac{k_{R\rightarrow IM2a}}{k_{IM2a\rightarrow R}} = \frac{[IM2a]}{[C_{10}H_8][OH^\bullet]} \quad (9)$$

$$K_c(2) = \frac{k_{R\rightarrow IM2b}}{k_{IM2b\rightarrow R}} = \frac{[IM2b]}{[C_{10}H_8][OH^\bullet]} \quad (10)$$

Therefore, the overall kinetics of the hydroxyl radical addition pathways on naphthalene does not depend upon the energy barriers characterizing the first bimolecular rate constants, but upon the Gibb's free energy differences between the reactants and the energized adducts [$C_{10}H_8OH^\bullet$] (IM1a, IM1b) as well as upon the energy barriers characterizing the subsequent unimolecular dissociation reaction steps (i.e. homolytic cleavages of C–H bonds). We correspondingly report in Tables 1 and 2 branching ratios, which were obtained according to:

$$R(1) = \frac{k_{eff}(1)}{k_{eff}(1) + k_{eff}(2)} \quad (11)$$

$$R(2) = \frac{k_{eff}(2)}{k_{eff}(1) + k_{eff}(2)} \quad (12)$$

At all pressures, the most abundant product resulting from the oxidation of naphthalene by OH radicals is 1-naphthol (P1). From these data, and the correspondingly computed regioselectivity indices [RSI= $R(1)$–$R(2)$, see Figure 5], we also note a decrease of the regioselectivity of the reaction with increasing temperatures and lowering pressures.

Table 3. Rate constants (units: unimolecular reactions in s^{-1}; bimolecular reactions in cm^3 $molecule^{-1}$ s^{-1}), effective rate constants, and branching ratios for the reported reaction channels by means of RRKM theory (P = 128 mbar).

T (K)	Rate constant						Effective rate constant		Branching ratio		k_{exp} [9,14,18]
	R→IM2a	R→IM2b	IM2a→R	IM2b→R	IM2a→P1	IM2b→P2	R→P1	R→P2	$R(1)$	$R(2)$	
300	3.87×10^{-15}	1.49×10^{-15}	2.87×10^{-2}	4.90×10^{-1}	1.47×10^{-6}	1.37×10^{-5}	1.98×10^{-19}	4.17×10^{-20}	82.63	17.37	$(18.6\pm1.0)\times10^{-12}$
337	3.26×10^{-15}	1.81×10^{-15}	1.28×10^{0}	1.57×10^{1}	1.59×10^{-4}	1.19×10^{-3}	4.05×10^{-19}	1.37×10^{-19}	74.69	25.31	$(14.6\pm5.0)\times10^{-12}$
358	3.02×10^{-15}	1.93×10^{-15}	7.84×10^{0}	8.16×10^{1}	1.48×10^{-3}	1.00×10^{-2}	5.70×10^{-19}	2.36×10^{-19}	70.68	29.32	$(11.0\pm4.4)\times10^{-12}$
378	2.85×10^{-15}	2.03×10^{-15}	3.65×10^{1}	3.32×10^{2}	9.91×10^{-3}	6.13×10^{-2}	7.74×10^{-19}	3.75×10^{-19}	67.37	32.63	$(10.1\pm4.0)\times10^{-12}$
407	2.64×10^{-15}	2.10×10^{-15}	2.61×10^{2}	1.98×10^{3}	1.13×10^{-1}	6.23×10^{-1}	1.14×10^{-18}	6.61×10^{-19}	63.36	36.64	$(10.5\pm4.0)\times10^{-12}$

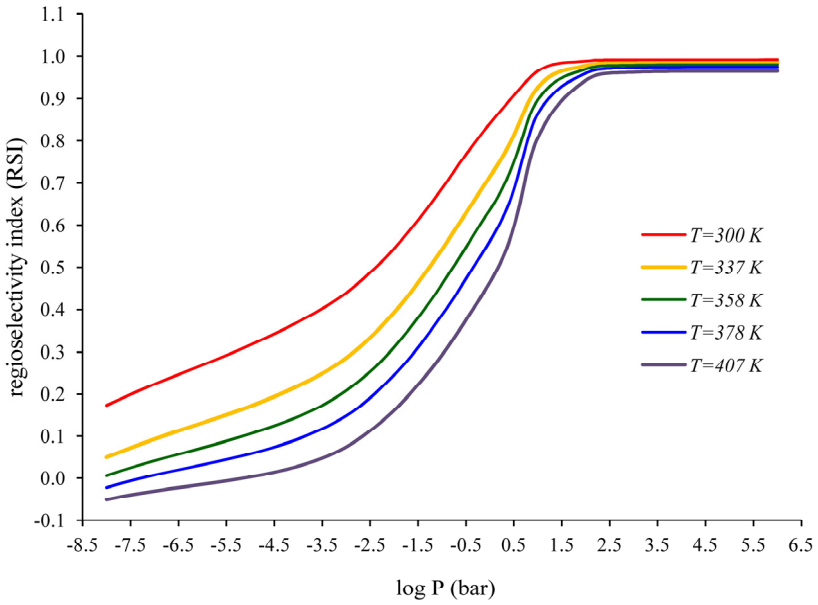

Figure 5. Dependence upon the pressure and temperature of the regioselectivity [RSI = $R(1)$–$R(2)$] of OH radical addition on naphthalene, according to the RRKM estimates of effective rate constants [$k_{eff}(1)$, $k_{eff}(2)$] supplied in Tables S4a–S4j (see Supporting Information).

From Figure 6 and Table 3, it is clear that, at the experimental pressure of 128 mbar, the RRKM rate constants obtained from the CBS-QB3 energy profiles for the R→IM2a reaction step along the chemical pathway leading to 1-naphthol underestimate the experimental ones by about two orders of magnitude. The overall rate constants reported in Table 3 for the formation of 1-naphthol or 2-naphthol indicate that this reaction is too slow to compete with

further reaction channels. Most likely, removal of the intermediate adducts IM2a and IM2b is to be ascribed to recombination with further OH radicals.

TST and RRKM data at 1 bar are not all strictly equal, indicating that the high pressure limit has not been reached at this pressure for all reaction channels. The high pressure limit for the IM2x→Px, IM2x→R and IM1→IM2b reaction steps is reached within 1% accuracy when the pressure exceeds 10^{-4}, 10^{-3} and 10^{2} bar, respectively, whatever the temperature (see Figure 6). These observations can be correlated with energy barriers equal to 28.2 or 29.4 kcal mol^{-1}, 21.4 or 19.4 kcal mol^{-1}, and 3.5 kcal mol^{-1}, respectively. In line with an effective negative energy barrier (-1 kcal mol^{-1}), this is only at a pressure of 10^{3} bar that some convergence to the high pressure limit starts to be seen for the IM1→IM2a reaction step. Pressures larger than 10^{5} bar are required for restoring the validity of the transition state approximation for the first bimolecular reaction steps within ~5 % accuracy. Besides the low or even negative energy barriers, such a high pressure value may also be the consequence of the large molecular volume of the reactant and the extent of the depth (~100 kJ/mol) of the interaction well between naphthalene and hydroxyl radicals.

3.3. Natural bond orbital (NBO) analysis

The extent of donor-acceptor interactions has been estimated by second-order perturbation theory. For each donor NBO(i) and acceptor NBO(j), the stabilization energy (E_2) associated with the $i \rightarrow j$ delocalization is obtained using:

$$E_2 = \Delta E_{ij} = q_i \left[\frac{F_{(i,j)}^2}{\varepsilon_i - \varepsilon_j} \right] \qquad (13)$$

where q_i is the donor orbital occupancy, ε_i and ε_j are diagonal elements (orbital energies) of the NBO Fock matrix, and $F_{(i,j)}$ are off-diagonal elements of this matrix.

The NBO data reported in Table 4 for the TS1a and TS1b transition states reveals that a very strong interaction prevails in between one of the oxygen lone pairs of the hydroxyl radical and the unoccupied $\pi^*(C_1–C_2)$ orbital. The corresponding stabilization energies range from 8.9 to 14.2 kcal mol^{-1}. The NBO analysis demonstrates that anomeric [$n_O \rightarrow \sigma^*_{C1–C2}$] and hyperconjugative [$n_O \rightarrow \pi^*_{C1–C2}$] interactions have a significant influence on activation and reaction energies.

Table 4. NBO occupancies and stabilization energies (in kcal mol^{-1}) characterizing intermediate and transition structures along the chemical reaction pathways **1** and **2** (results obtained at the B3LYP/6-311G(2d,d,p) level of theory).

	B3LYP/6-311G(2d,d,p)			
	IM2a	IM2b	TS1a	TS1b
Occupancies				
$\sigma(C_1–C_2)$	0.9902	0.9906	0.9902	0.9904
$\sigma^*(C_1–C_2)$	0.0149	0.0140	0.0071	0.0071
$\pi(C_1–C_2)$	-	0.8116	0.8499	0.8584
$\pi^*(C_1–C_2)$	-	0.4909	0.1426	0.1532
$n_{O(1)}$	0.9923	0.9925	0.9983	0.9983
$n_{O(2)}$	0.9792	0.9800	0.9922	0.9898
$n_{O(3)}$	-	-	0.9587	0.9411
Stabilization energies (E_2)				
$n_{O(1)} \rightarrow \sigma^*(C_1–C_2)$	3.28	3.27	-	0.03
$n_{O(1)} \rightarrow \pi^*(C_1–C_2)$	-	5.08	0.97	1.48
$n_{O(2)} \rightarrow \pi^*(C_1–C_2)$	-	1.03	-	0.16
$n_{O(3)} \rightarrow \pi^*(C_1–C_2)$	-	-	8.88	14.17

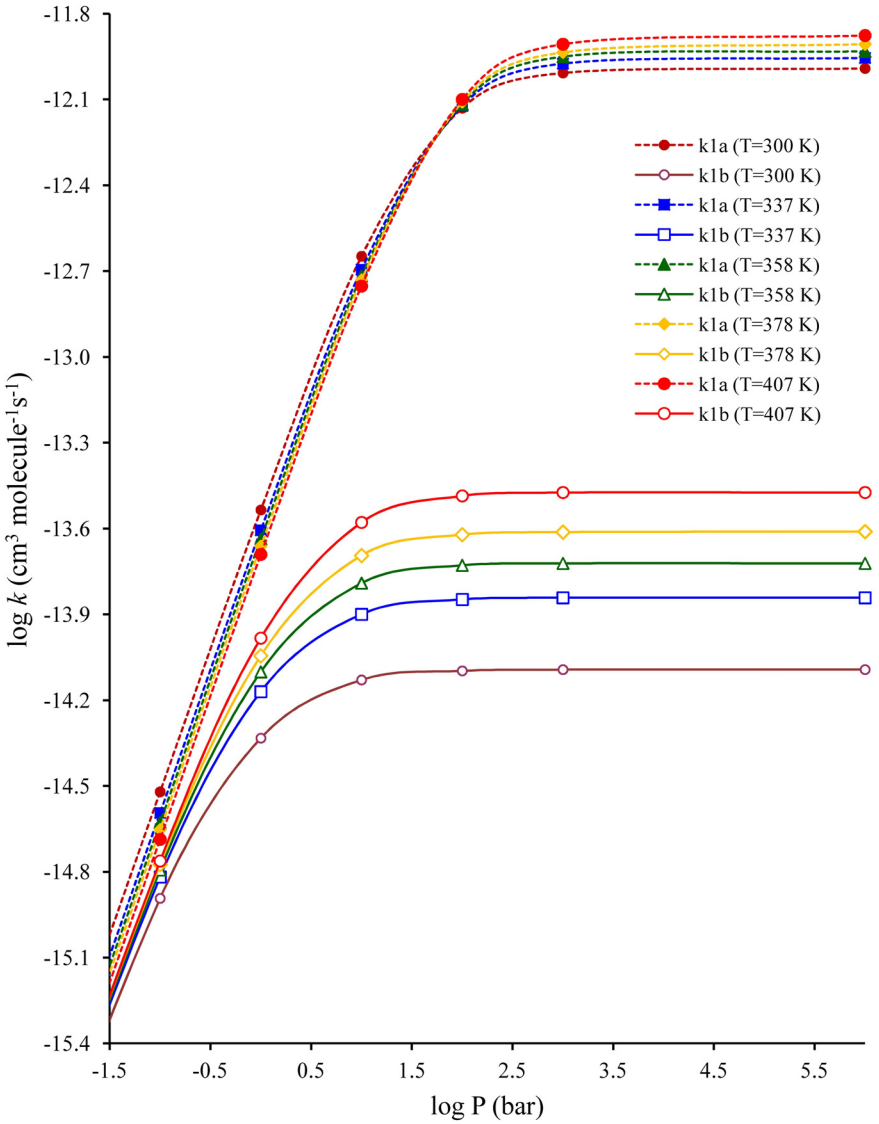

Figure 6: Pressure dependence of the bimolecular rate constants for the R→IM2a (k1a) and R→IM2b (k1b) reaction steps (RRKM results, obtained by means of eq. 3).

4. CONCLUSIONS

The available experimental kinetic rate constants for the reaction between naphthalene and OH radicals under inert conditions and at temperatures lower than 410 K correspond to a bimolecular reaction step leading to a molecular energized adduct [$C_{10}H_8OH^{\bullet}$]. This first reaction step is strongly exergonic at ambient temperature and pressure. In line with experiment, due to the formation of a pre-reactive Van der Waals (VdW) molecular complex [$C_{10}H_8\cdots OH$]$^{\bullet}$, the corresponding transition state lies below the reactant, hence an effective negative activation energy around −1.5 kcal mol^{-1} on the reaction pathway leading to 1-naphthol. In contrast, on the reaction pathway leading to 2-naphthol, the first bimolecular reaction step is characterized by a positive activation energy, around 1 kcal mol^{-1}. The formation of the energized adduct is followed by a unimolecular reaction step which is strongly endergonic at ambient temperature and pressure, and which corresponds to the elimination of a H-atom (H$^{\bullet}$), yielding 1- or 2-naphthol.

Effective rate constants have been calculated according to a steady state analysis upon a two-step model reaction mechanism, assuming reversibility of the first bimolecular addition reaction step, and irreversibility of the second unimolecular dissociation step. In line with experiment, the obtained branching ratios indicate that the most abundant product resulting from the oxidation of naphthalene by OH radicals must be 1-naphthol. The regioselectivity of this reaction decreases with increasing temperatures and decreasing pressures.

The transition-state-approximation breaks down at 1 bar for the first bimolecular reaction steps. This is particularly true for the first bimolecular reaction step involved in the $OH^{\bullet}$ addition pathway leading to 1-naphthol, which is characterized by an effective activation energy of −1.5 kcal mol^{-1}. RRKM calculations show that overwhelmingly high pressures, larger than 10^5 bar, are required for restoring within ~5 % accuracy the validity of this approximation for *all* reaction channels in the OH addition pathway, in particular for the conversion of the pre-reactive Van der Waals complex $[C_{10}H_8\cdots OH]^{\bullet}$ into the molecular energized adduct $C_{10}H_8OH^{\bullet}$.

NICS indices and natural bond orbital analysis also show that the computed activation and reaction energies are largely dictated by alterations of aromaticity and, to a lesser extent, by anomeric and hyperconjugative effects pertaining to the delocalization of oxygen lone pairs to neighboring empty σ^*_{C1-C2} and π^*_{C1-C2} orbitals.

Reference

[1] A. Shiroudi, M.S. Deleuze and S. Canneaux, J. Phys. Chem. A, *118* (**2014**) 4593.